on MT detoxification of toxic heavy metals, including mercury. In our study, we induced anti-MT antibodies by immunization with MT in BALB/c mice and investigated the toxic effects of mercury on bone and immune system. Our results demonstrate that anti-MT antibody induction causes $HgCl_2$-induced bone injury and enhances $HgCl_2$-induced immune disorders.

MATERIALS AND METHODS

Mice. Specific pathogen-free male BALB/c (H-2^d) mice were purchased from Japan SLC (Hamamatsu, Japan). Mice were kept in specific pathogen-free conditions with 12-h dark and 12-h light cycles, given standard rodent chow and tap water *ad libitum*.

MT immunization and mercury treatment. Eight-week-old mice were randomly divided into control, MT immunization (anti-MT Ab), MT immunization plus $HgCl_2$ treatment ($HgCl_2$ + anti-MT Ab), and $HgCl_2$ treatment ($HgCl_2$) groups. In a parallel experiment, anti-MT Ab levels in the serum were measured.

MT (Sigma Chemical Co., St. Louis, MO) containing MT-I and MT-II from rabbit liver was dissolved in sterile 0.9% NaCl and emulsified with an equal volume of Freund's complete adjuvant (FCA). One hundred microliters of mixture was injected intracutaneously (ic) into a foot-pad at a dose of 10 μg of MT per mouse. After 1 week, mice were boosted with injection of antigen four times every 2 weeks. Control and $HgCl_2$ treatment groups received the same immunization mixture of 0.9% NaCl and FCA (ic).

$HgCl_2$ (Sigma) was prepared in sterile 0.9% NaCl. One week after the end of MT immunization, mice received subcutaneous injections of 1 mg/kg of $HgCl_2$, three times per week for 1, 2, and 3 weeks. Control and MT immunization groups received only 0.9% NaCl (sc).

BMD measurement. Bone mineral density was measured by dual-energy X-ray absorptiometry (DEXA) using a PIXImus mouse densitometer (Lunar Corp., Madison, WI). Four experimental groups of mice were placed on a plastic attenuator under slight ether anesthesia at a time from 1 to 3 weeks after $HgCl_2$ treatment. They were scanned as spine and femur using software version 1.46. The result of BMD was expressed as bone mineral content (BMC)/area (mg/cm^2).

Blood and organ collection. Mice were bled for baseline anti-MT titers by retro-orbital puncture under slight ether anesthesia 1 day before MT immunization. Four experimental groups of mice were bled as described above following DEXA analysis and then euthanized by cervical dislocation. Their spleens, livers, and kidneys were removed. The blood from each mouse was allowed to clot at 4°C. The serum was separated after centrifugation and stored at −80°C until assayed.

Anti-MT Ab detection. Anti-MT Ab in serum was determined by a sandwich ELISA. Microplates (Sumitomo, Japan) were coated with 50 μl of MT at a concentration of 4 μg/ml in coating buffer (carbonate buffer, pH 9.8) and overnight incubation at 4°C. Plates were blocked with 1% bovine serum albumin in phosphate-buffered saline at room temperature. Diluted sera (1: 2000) were added to the wells in duplicate and the plates were incubated at RT for 1 h. The plates were then washed with washing buffer (PBS/0.05% Tween-20) and diluted (1/1000, in PBS with 1% BSA) horseradish peroxidase-conjugated rat anti-mouse IgG1 (clone X56) or IgG2a (clone R19-15) mAbs (PharMingen, San Diego, CA) was added to the wells and incubated for 1 h at RT. The plates were washed. Thereafter, tetramethylbenzidine and hydrogen peroxide substrate reagent (PharMingen) were added to wells. After incubation at RT for 20 min, the reaction was stopped by 1 M H_3PO_4. The absorbance was measured within 30 min at 450 nm by a microplate reader (Bio-Rad model 550).

Mercury detection. Serum mercury concentration was measured by the thermal decomposition, gold amalgamation, and cold vapor atomic absorption method (SP-3 Mercury Analyzer; Nippon Instruments, Tokyo, Japan). The detection limit of this method was 0.2 μg/dl. Mercury levels in liver and kidney were measured by the inductively coupled plasma spectrometry method. Accurately measured samples of liver and kidney were digested in 13.1 M distilled HNO_3 by the Microwave Digestion System (Ethos Plus; Milestone, Bergamo, Italy). Concentrated acid mixture [KI/HCl, 2:10 (v/v)] was then added to the digests and heated (5 min, 70°C). The digests were quantified with 1% HCl, and mercury content was measured with an ICPS7500 Sequential Plasmaspectrometer and HVG-ICP Hydride Vapor Generator (Shimadzu Corp., Kyoto, Japan). The detection limit of this method was 0.05 μg/g.

Western blot analysis. Portions of liver and kidney were disrupted by an ultrasonicator in ice-cold Nonidet P-40 lysis buffer (Urano *et al.*, 2000). The lysate was then centrifuged at 15,000 rpm for 20 min at 4°C. Protein concentration in the lysate was measured using the Bio-Rad assay dye reagent concentrate (Bio-Rad). The extracted proteins were boiled for 5 min, and 80 μg protein per lane was subjected to SDS–polyacrylamide gel electrophoresis using a 15% running gel and blotted onto a Sequi-Blot PVDF Membrane (Bio-Rad). After reacting the membranes with anti-MT mAb (StressGen, Victoria, British Columbia, Canada), the detection step was performed using ECL Western blotting detection reagents (Amersham Pharmacia Biotech) according to the manufacturer's protocol.

Spleen cell suspension. Single cell suspensions of spleen were resuspended in Tris–NH_4Cl hemolysis buffer to remove red blood cells. The cells were then washed with RPMI 1640 (Gibco BRL) and resuspended in PBS for flow cytometry analysis or in RPMI 1640 medium containing 10% heat-inactivated fetal bovine serum (JRH Biosciences), 100 U/ml of penicillin, and 100 μg/ml of streptomycin for cytokine assays.

Flow cytometry analysis of lymphocytes. Spleen cells were double stained with fluorescein isothiocyanate (FITC)-conjugated rat anti-mouse CD19 (clone 1D3) and phycoerythrin (PE)-conjugated hamster anti-mouse CD3 (clone 145-2C11) mAbs (PharMingen) for 40 min at 4°C in a dark place. Cells were washed and analyzed by flow cytometry using an EPICS Elite apparatus (Coulter Electronics, Hialeah, FL). A fluorescein histogram of 10,000 counts was collected for each sample.

Cytokine assays. Splenic lymphocytes (2×10^6 per well) were stimulated by 1 μg/ml of purified hamster anti-mouse CD3 mAb (clone 145-2C11; PharMingen) for interleukin-4 (IL-4), IL-10, and interferon-γ (IFN-γ) or stimulated by 10 μg/ml of lipopolysaccharide (LPS, *Escherichia coli* serotype 0127:B8; Sigma) for IL-12 measurements, in 24-well culture plates (Falcon, Becton-Dickinson, Rutherford, NJ). After incubation for 24 h at 37°C in a humidified 5% CO_2 incubator, the supernatants were collected and assayed for cytokine secretion by ELISA (Biosource International) in duplicate according to the manufacturer's protocol.

ELISA for serum IgE and IgG subclasses. Total serum IgE and IgG subclasses were determined by an ELISA method. In this experiment, we used Mouse IgE OptEIA Set (PharMingen) for IgE and Mouse IgG ELISA Quantitation Kit (Bethyl Laboratories Inc.) for IgG1, IgG2a, and IgG2b measurements, according to the manufacturer's protocol, respectively. Sera were diluted serially and added to wells in duplicate. Absorbance values were measured at 450 nm.

Detection of serum calcium, alkaline phosphatase, and osteocalcin. Serum calcium concentrations and alkaline phosphatase (ALP) activity were determined using an autoanalyzer (Hitachi 7170). Serum levels of osteocalcin were determined by a two-site sandwich enzyme radioimmunoassay using goat anti-mouse osteocalcin (Biomedical Technological Inc., Stoughton, MA) according to the manufacturer's protocol.

Histological analysis. Formalin-fixed portions of liver were embedded in paraffin and cut at a 5-μm thickness. Sections were then stained with hematoxylin, phloxine, and eosin (H & E). Histopathological evaluation of liver was observed under light microscopy.

Statistical analysis. The results were expressed as mean ± SE. Statistical analyses were performed using multivariate one-way ANOVA followed by Fisher's Protected LSD test, using StatView software for Macintosh. A value of $p < 0.05$ was considered to indicate a significant difference in all statistical analyses.

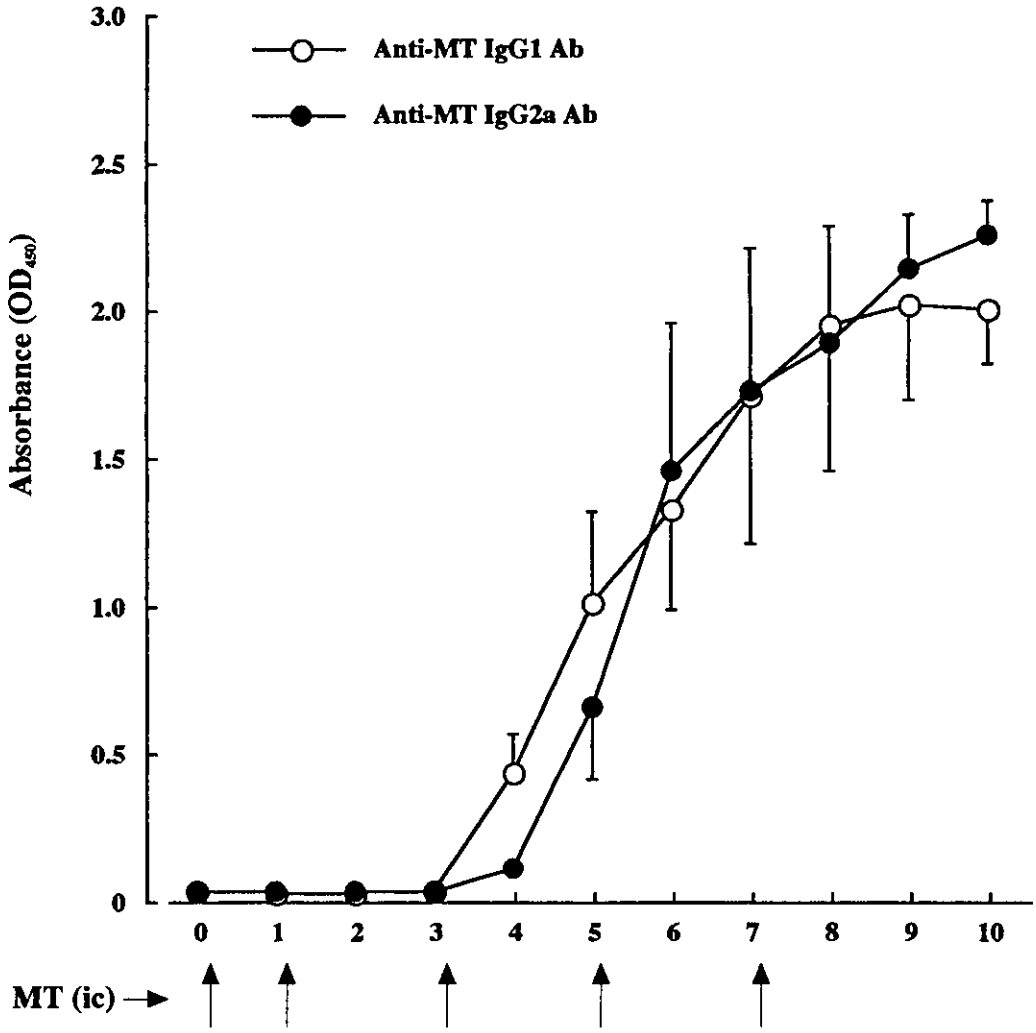

FIG. 1. Induction of anti-MT Ab by immunization of MT (10 μg/mouse) in BALB/c mice. MT was dissolved in 0.9% NaCl and emulsified with an equal volume of FCA. The mixture was repeatedly (arrows) injected (ic) into a foot-pad. Mice were bled by retroorbital puncture under slight ether anesthesia. Serum levels of anti-MT IgG1 and IgG2a Ab were measured by using an ELISA method. Data are shown as means ± SE (n = 8).

RESULTS

Anti-MT Ab Induction in Mice

To induce anti-MT Ab, BALB/c mice were immunized (ic) five times with MT. Serum levels of anti-MT IgG1 and IgG2a Abs were measured by an ELISA method. Anti-MT IgG1 and IgG2a Abs were detectable at 4 weeks and were greatly induced approximately 6 weeks after MT immunization (Fig. 1).

MT Immunization plus $HgCl_2$ Treatment Decreases BMD

In this experiment, we investigated the effect of MT immunization and $HgCl_2$ treatment on BMD using a DEXA method at different weeks after the start of $HgCl_2$ injection (sc). Both $HgCl_2$ treatment alone and MT immunization did not affect the BMD value in the whole period of this experiment. Nevertheless, MT immunization plus $HgCl_2$ treatment dramatically decreased femoral BMD after 2 weeks of $HgCl_2$ injection and also decreased spinal BMD at week 3 (Fig. 2). These results indicate that $HgCl_2$ alone does not affect mouse BMD, but if an immune response to MT is induced in mice, bone is injured by $HgCl_2$.

Serum Changes in Bone Parameters

We then examined serum calcium concentration, ALP activity, and osteocalcin level that related to bone metabolism after 3 weeks of $HgCl_2$ injection. No differences were seen in

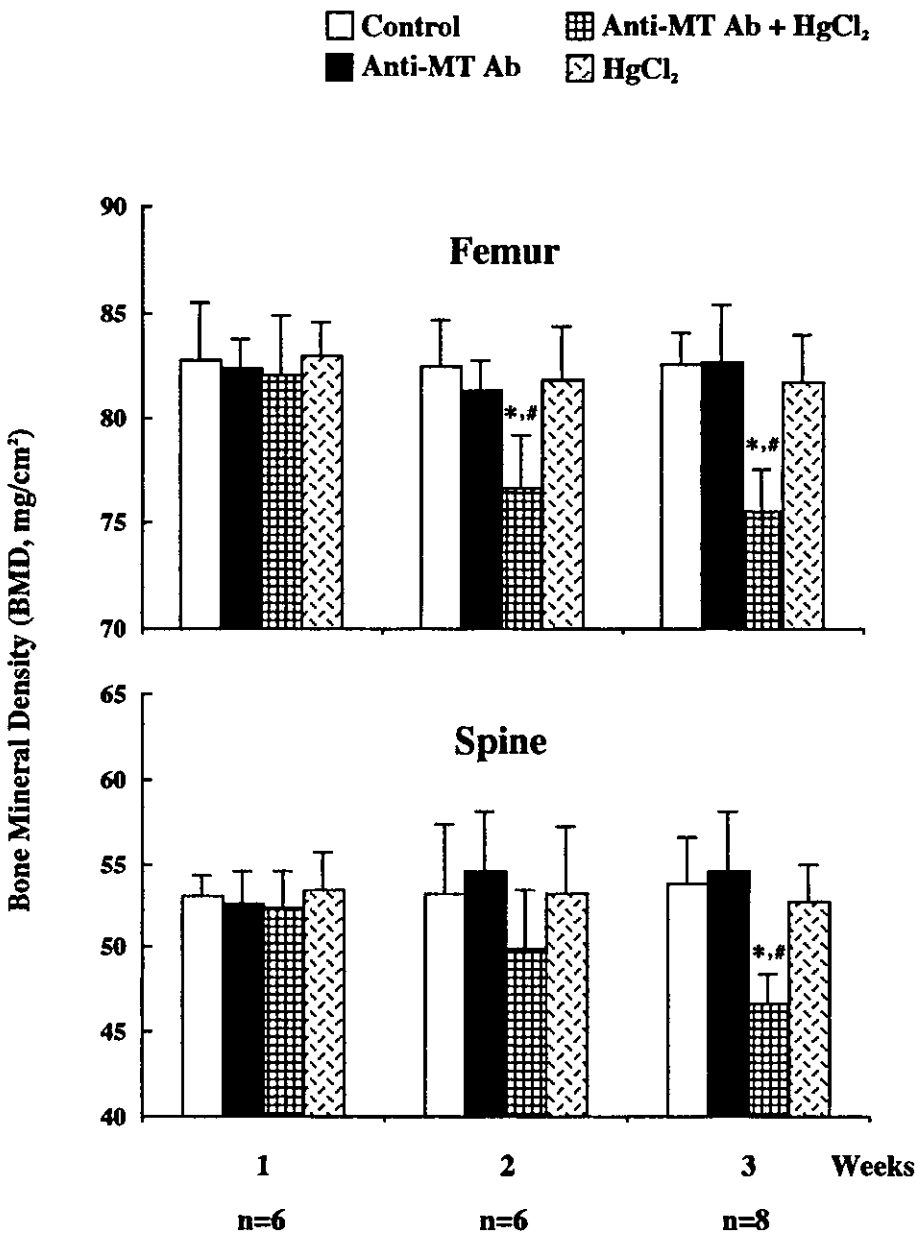

FIG. 2. MT immunization plus $HgCl_2$ treatment decreased BMD. Mice were immunized with MT same as described in the legend to Fig. 1. Control and $HgCl_2$ treatment groups received the same immunization mixture of 0.9% NaCl and FCA (ic). One week after the end of MT immunization, mice were injected with $HgCl_2$ (1 mg/kg sc) three times per week. Control and MT immunization groups received only 0.9% NaCl (sc). The spine and femur BMD were measured by using dual-energy X-ray absorptiometry. Data are expressed as means ± SE. * $p < 0.05$, compared with control group; # $p < 0.05$, compared with $HgCl_2$ group.

serum calcium concentration among the four groups. However, serum ALP activity and osteocalcin level were significantly decreased in MT immunization plus $HgCl_2$ treatment group compared to those of other groups in accordance with the results of BMD (Fig. 3).

MT Immunization Changes Mercury Distribution

The effect of MT immunization on mercury distribution was analyzed at 3 weeks of $HgCl_2$ injection. Mercury levels in serum and liver were significantly increased and kidney

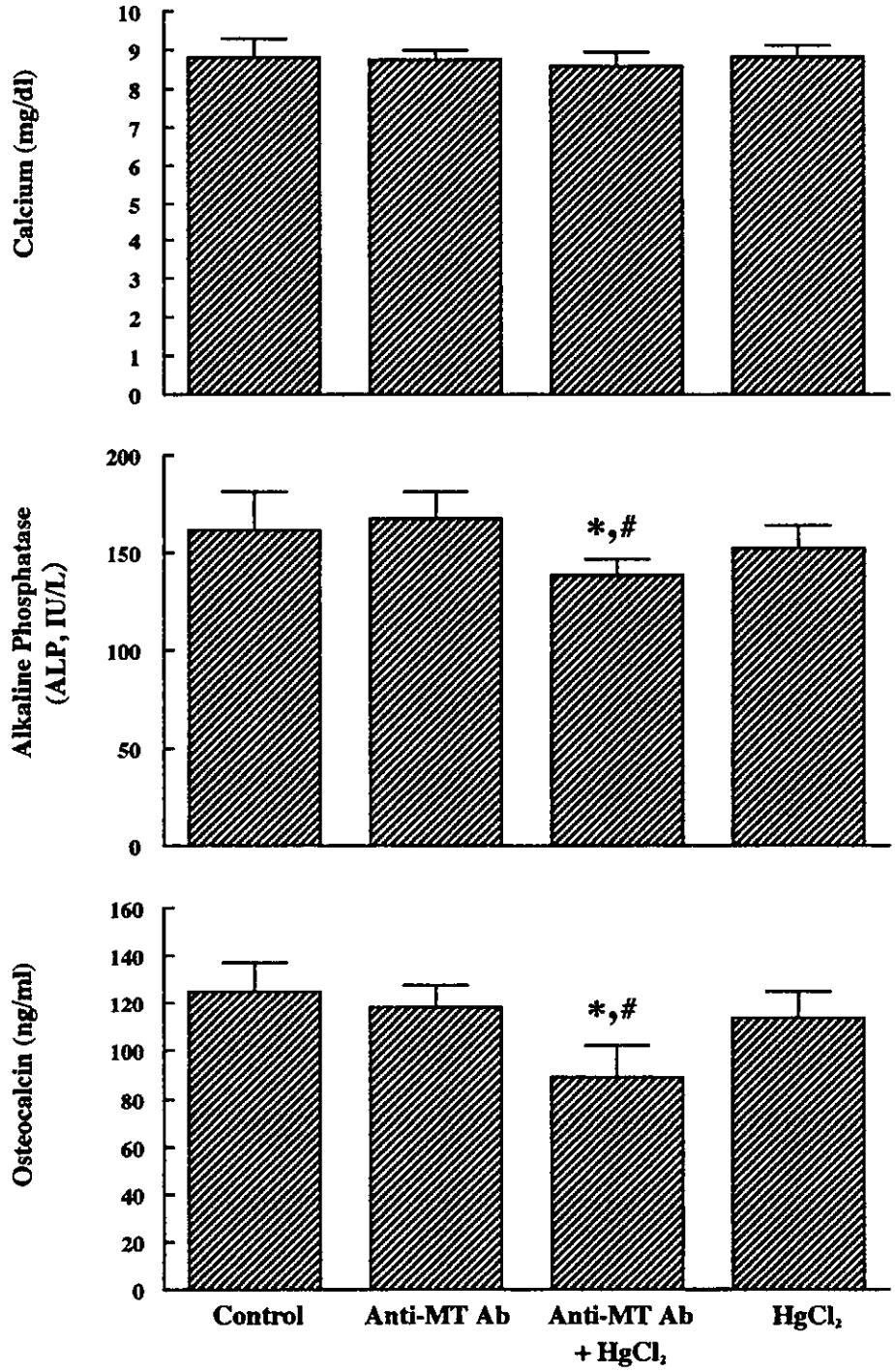

FIG. 3. MT immunization plus $HgCl_2$ treatment decreased serum ALP activity and osteocalcin level. Serum calcium concentrations and ALP activity were determined using an autoanalyzer, and serum levels of osteocalcin were determined using a two-site sandwich enzyme radioimmunoassay method, at 3 weeks of $HgCl_2$ injection. Data are shown as means ± SE ($n = 8$). * $p < 0.05$, compared with control group; # $p < 0.05$, compared with $HgCl_2$ group.

mercury level was decreased, after MT immunization plus $HgCl_2$ treatment, compared to $HgCl_2$ treatment alone (Fig. 4). There was no detectable mercury in control or MT-immunized mice.

MT Immunization Impedes $HgCl_2$-Induced Increase of MT Expression in Liver

Mercury can induce MT synthesis in the liver and kidney, so we investigated the effect of MT immunization and $HgCl_2$

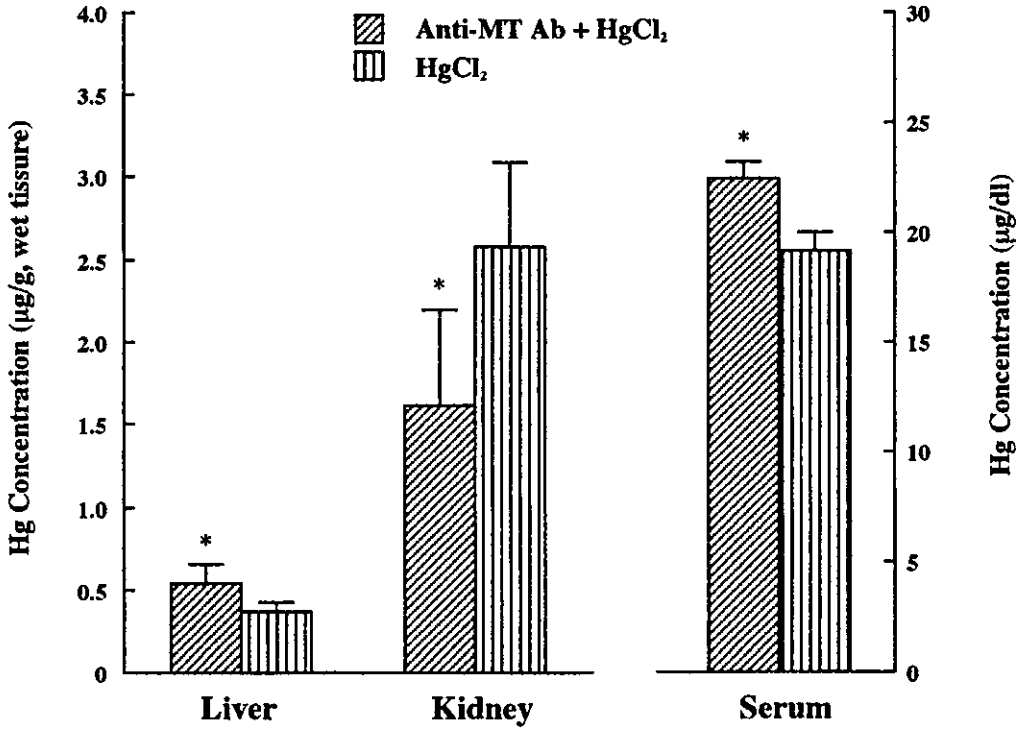

FIG. 4. Effects of MT immunization on distribution of mercury in serum, liver, and kidney at 3 weeks of $HgCl_2$ injection. Mercury concentrations in serum and tissues were measured by using a cold vapor atomic absorption method and inductively coupled plasma spectrometry method, respectively. Data are shown as means ± SE ($n = 6$). * $p < 0.05$, compared with $HgCl_2$ group.

treatment on MT expression in the liver and kidney by the Western blot method. As shown in Fig. 5, $HgCl_2$ treatment led to remarkable MT expression in the liver and kidney, but MT immunization did not affect mercury-induced increase of MT expression in the kidney. However, it clearly impeded mercury-induced MT synthesis in the liver.

Histological Changes in Liver

The effects of MT immunization and $HgCl_2$ treatment on histological changes in the liver were also investigated. Sections of liver from the control mice were morphologically unremarkable (Fig. 6A). However, livers from MT-immunized mice exhibited remarkable fatty metamorphosis focusing on the central vein and some destroyed liver architecture (Fig. 6B). Treatment of $HgCl_2$ for 3 weeks destroyed normal liver structure with degeneration of hepatocytes (Fig. 6D). Meanwhile, livers from mice of MT immunization plus $HgCl_2$ treatment showed remarkably fatty metamorphosis, serious destroyed liver architecture with degeneration as well as necrotic change of hepatocytes, and vasodilation (Fig. 6C).

Anti-MT Ab Induction Enhances $HgCl_2$-Induced Increase in Total Serum Levels of IgE and IgG1

As shown in Fig. 7, serum levels of IgG1 and IgE were significantly increased in the $HgCl_2$ treatment group compared to those in the control group at week 2 and week 3, respectively. There were no differences in serum levels of IgE and IgG subclasses between MT immunization and control group. MT immunization and/or $HgCl_2$ treatment had no effect on serum level of IgG2b; whereas MT immunization significantly enhanced $HgCl_2$-induced increases in serum levels of IgG1 and IgE compared with $HgCl_2$ treatment and markedly increased serum level of IgG2a, just 2 weeks after $HgCl_2$ injection. These results indicate that anti-MT Ab induction enhances $HgCl_2$-induced immune disorders relating to increased serum levels of IgE and IgG1.

Effects of MT Immunization and $HgCl_2$ Treatment on Splenic Expressions of T and B Cells

The effects of MT immunization and $HgCl_2$ treatment on splenic expressions of T and B cells were also examined by flow cytometry analysis. The MT immunization treatment group showed a significant increase of CD3 cells and a decrease of CD19 cells compared to those of control group. On the contrary, $HgCl_2$ treatment group showed an increase of CD19- and a decrease of CD3-positive cell percentages from week 2. There were no differences in CD3- and CD19-positive cell percentages between the $HgCl_2$ treatment group and the MT immunization plus $HgCl_2$ treatment group (Fig. 8).

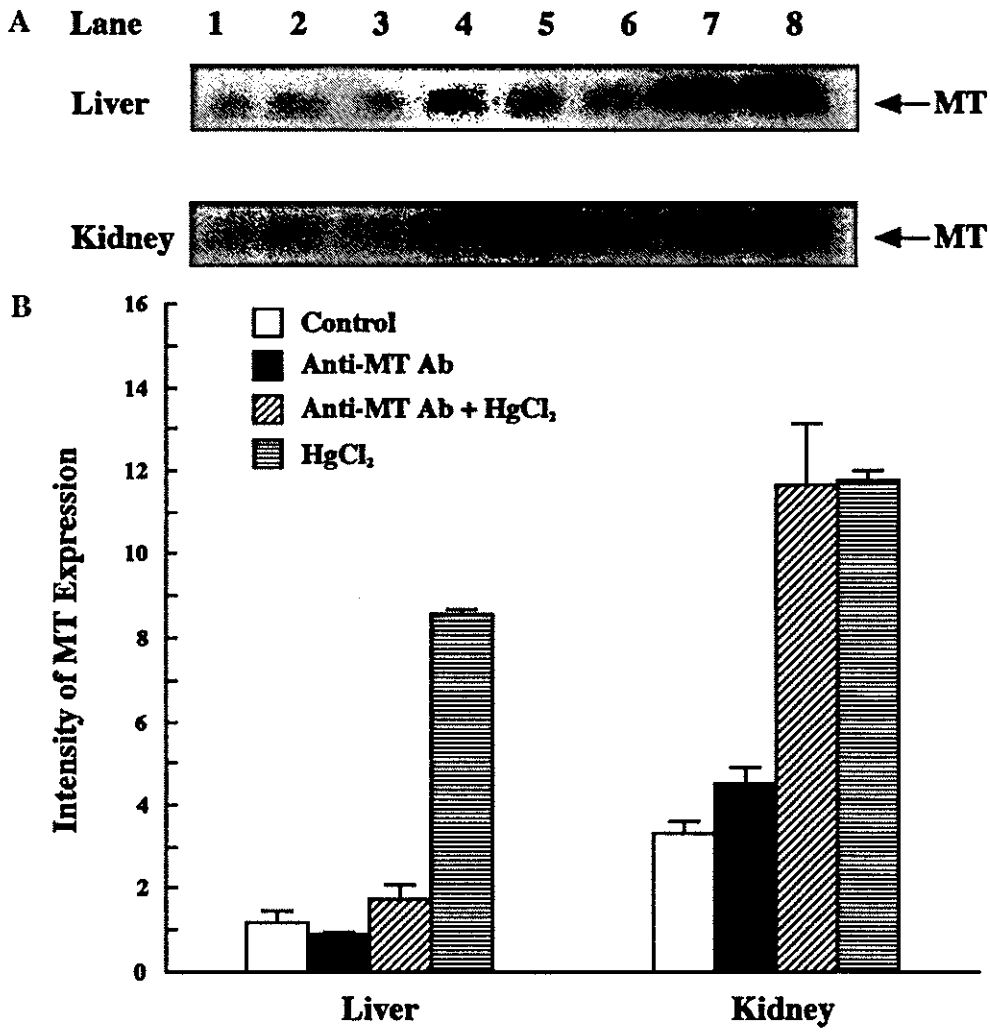

FIG. 5. Effects of MT immunization and $HgCl_2$ treatment on MT expression in liver and kidney. (A) MT expressions in liver and kidney at 3 weeks of $HgCl_2$ injection were detected by Western blot assay. Lanes 1 and 2, control; lanes 3 and 4, MT immunization; lanes 5 and 6, MT immunization plus $HgCl_2$; lanes 7 and 8, $HgCl_2$. (B) Intensity of MT expression was quantified by densitometer. Results are shown as means ± SE.

Anti-MT Ab Induction Enhances $HgCl_2$-Induced Increase of IL-4 and IL-10 Cytokine Production

Several studies have shown that $HgCl_2$ can elicit IL-4 production both *in vivo* and *in vitro* (Oliveira *et al.*, 1995; Prigent *et al.*, 1995; Dastych *et al.*, 1999; Gorrie *et al.*, 2000). Splenocytes were *in vitro* stimulated with anti-CD3 Ab or LPS, and cytokine production in the supernatants was determined by an ELISA method. MT immunization alone did not affect cytokine production. There were no differences in IL-12 and IFN-γ secretions among the four groups. However, splenocyte secretions of IL-4 and IL-10 from $HgCl_2$-injected mice at week 3 were significantly augmented compared to those of control mice. Moreover, IL-4 and IL-10 secretions were significantly increased by MT immunization plus $HgCl_2$ compared to the $HgCl_2$ treatment group, from 2 and 3 weeks after $HgCl_2$ injection (Fig. 9).

DISCUSSION

In susceptible animals, $HgCl_2$ induces a systemic autoimmune disease characterized by a T cell-dependent polyclonal B cell activation, increased serum levels of IgG1 and IgE, production of ANoA, and formation of immune complexes in the kidneys. Genetic analysis shows the MHC class II region is mainly related to mercury-induced autoimmunity. H-2^s mice, such as SJL, B10.S, A.SW, are susceptible to mercury-induced autoimmunity (Hultman and Enestrom, 1992; Warfvinge *et al.*, 1995; Hultman *et al.*, 1996; Bagenstose *et al.*, 1998b; Abedi-Valugerdi and Möller, 2000). Recent study shows that H-2 genes mainly determine the susceptibility to mercury-induced ANoA production, whereas non-H2 genes control the susceptibility to and the severity of the B cell activation and renal IgG deposition (Abedi-Valugerdi and Möller, 2000). Usually, BALB/c mice (H-2^d) are regarded as moderately responsive to

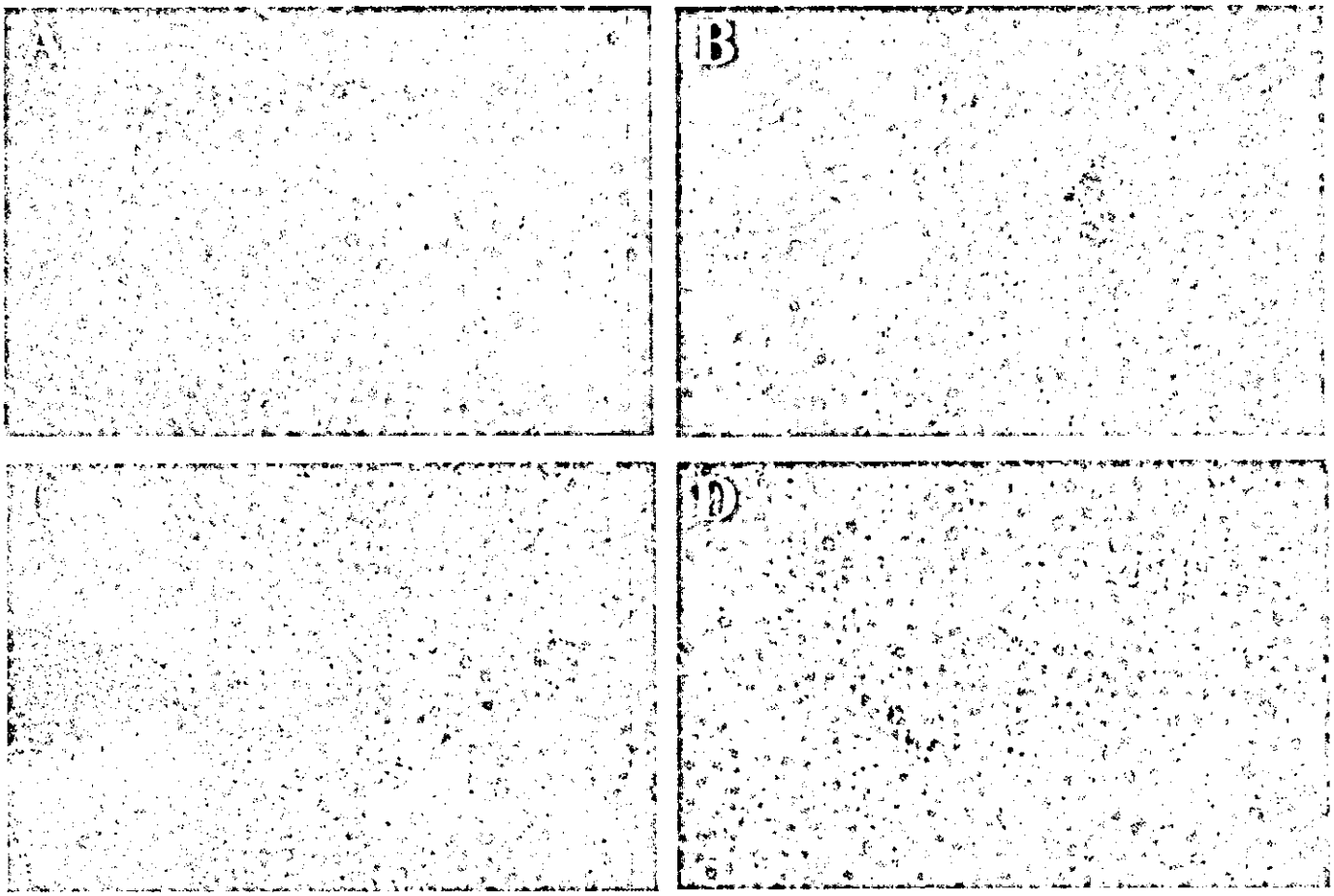

FIG. 6. Histopathological observations of MT immunization and $HgCl_2$ treatment. Liver sections were stained with H & E after 3 weeks of $HgCl_2$ injection. (A) Control; (B) MT immunization; (C) MT immunization plus $HgCl_2$; and (D) $HgCl_2$. Magnification 200×.

mercury. Our results show that $HgCl_2$-increased serum levels of IgE and IgG1 in BALB/c mice were similar to those of previous reports (Johansson *et al.*, 1998; Abedi-Valugerdi and Möller, 2000).

Although the exact mechanism for mercury-induced autoimmunity is not yet known, the increase of serum IgG1 and IgE in mercury-treated mice suggests that T helper (Th) 2 type cells play an important role in some pathogenesis of this syndrome. Mercury-treated IL-4-deficient mice had virtually no detectable serum IgG1 or IgE and very low levels of IgG1 ANoA, but these mice had similar levels of IgG2a and Ig2b class ANoA compared to IL-4 non-deficient mice, indicating IL-4 is required for the serum increase in IgG1 and IgE, but not for ANoA production in mercury-induced autoimmunity (Bagenstose *et al.*, 1998a). Moreover, IFN-γ treatment can partially prevent the mercury-induced increase in serum IgE but not affect the formation of ANoA (Doth *et al.*, 1997). More evidence that Th2 type immune responses play an important role in mercury-induced autoimmunity is that mercury elicits IL-4 production both *in vivo* (Gillespie *et al.*, 1996; Gorrie *et al.*, 2000) and *in vitro* (Prigent *et al.*, 1995) in susceptible animals and also directly enhances IL-4 production by murine mast cells *in vitro* (Oliveira *et al.*, 1995; Dastych *et al.*, 1999; Wu *et al.*, 2001). In our study, when spleen cells were stimulated by anti-CD3 Ab *in vitro*, the production of IL-4 and IL-10, but not IFN-γ and IL-12, was significantly increased in $HgCl_2$-injected mice compared to control mice. These results suggest that Th2-type cytokines may also be involved in mercury-induced autoimmunity in BALB/c mice. In addition, mercury treatment results in a significant increase in splenic B cell numbers in susceptible mice (Bagenstose *et al.*, 1998b; Johansson *et al.*, 1998). In this report, we investigated the effect of $HgCl_2$ on the splenic percentages of T and B cells. Our results indicate that $HgCl_2$ treatment in BALB/c mice increases B cells while decreasing T cell percentages, suggesting mercury favors B cell differentiation and may be related to the increase in total serum levels of IgE and IgG1.

MT, which is a cysteine-rich intracellular protein demonstrating a high affinity for metals, plays an important cytoprotective effect against metal toxicity. In four isoforms of MT (MT I–IV), MT-I and MT-II are expressed in all tissues, primarily attributing itself to protection against metal toxicity

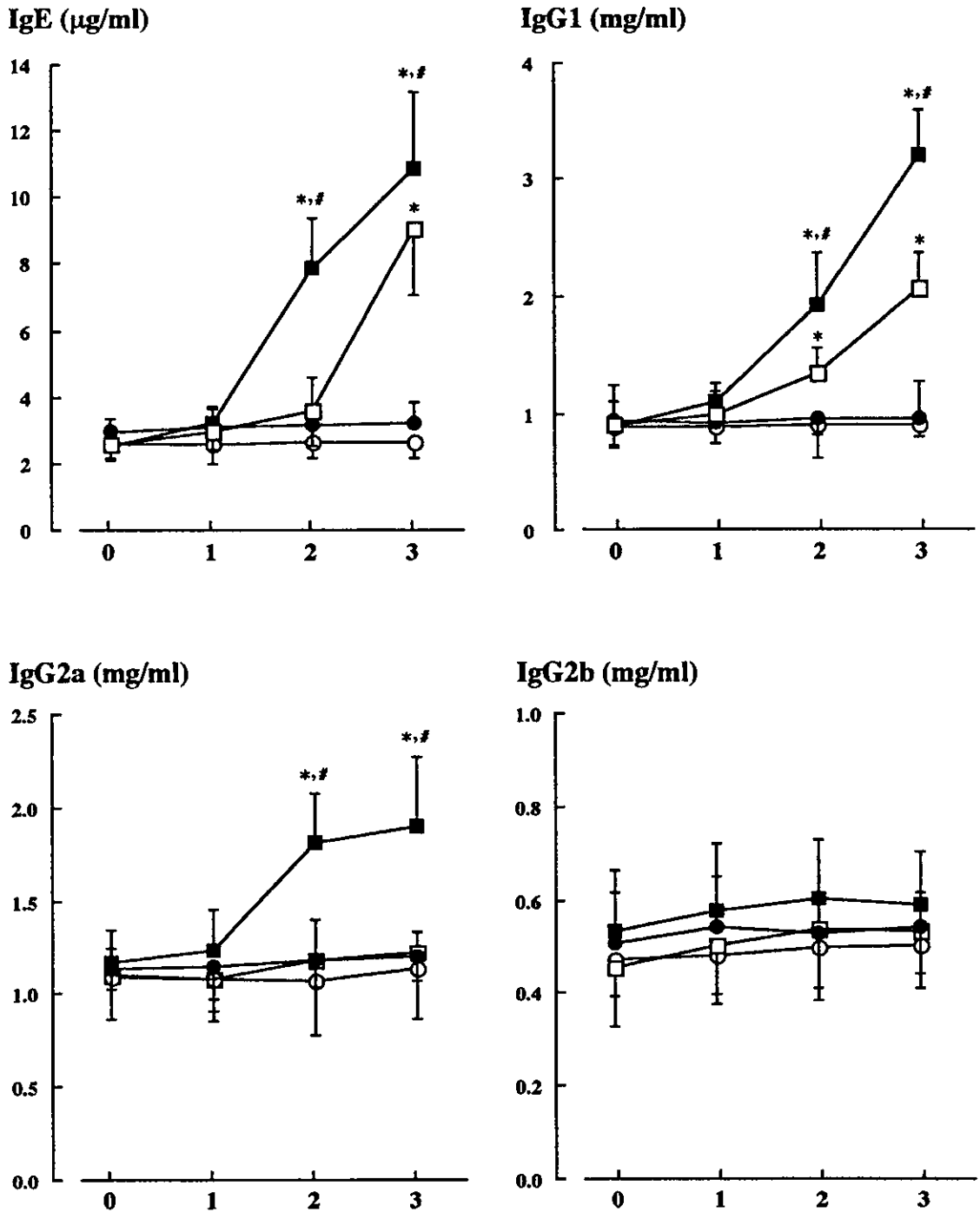

FIG. 7. MT immunization enhanced $HgCl_2$-induced increase of serum levels of IgE and IgG1. Mice of control (○), anti-MT Ab induction (●), anti-MT Ab induction plus $HgCl_2$ treatment (■), and $HgCl_2$ treatment (□), were bled by retroorbital puncture under slight ether anesthesia. Serum levels of IgE, IgG1, IgG2a, and IgG2b were tested using an ELISA method. Data points are shown as means ± SE ($n = 8$). * $p < 0.05$, compared with control group; # $p < 0.05$, compared with $HgCl_2$ group.

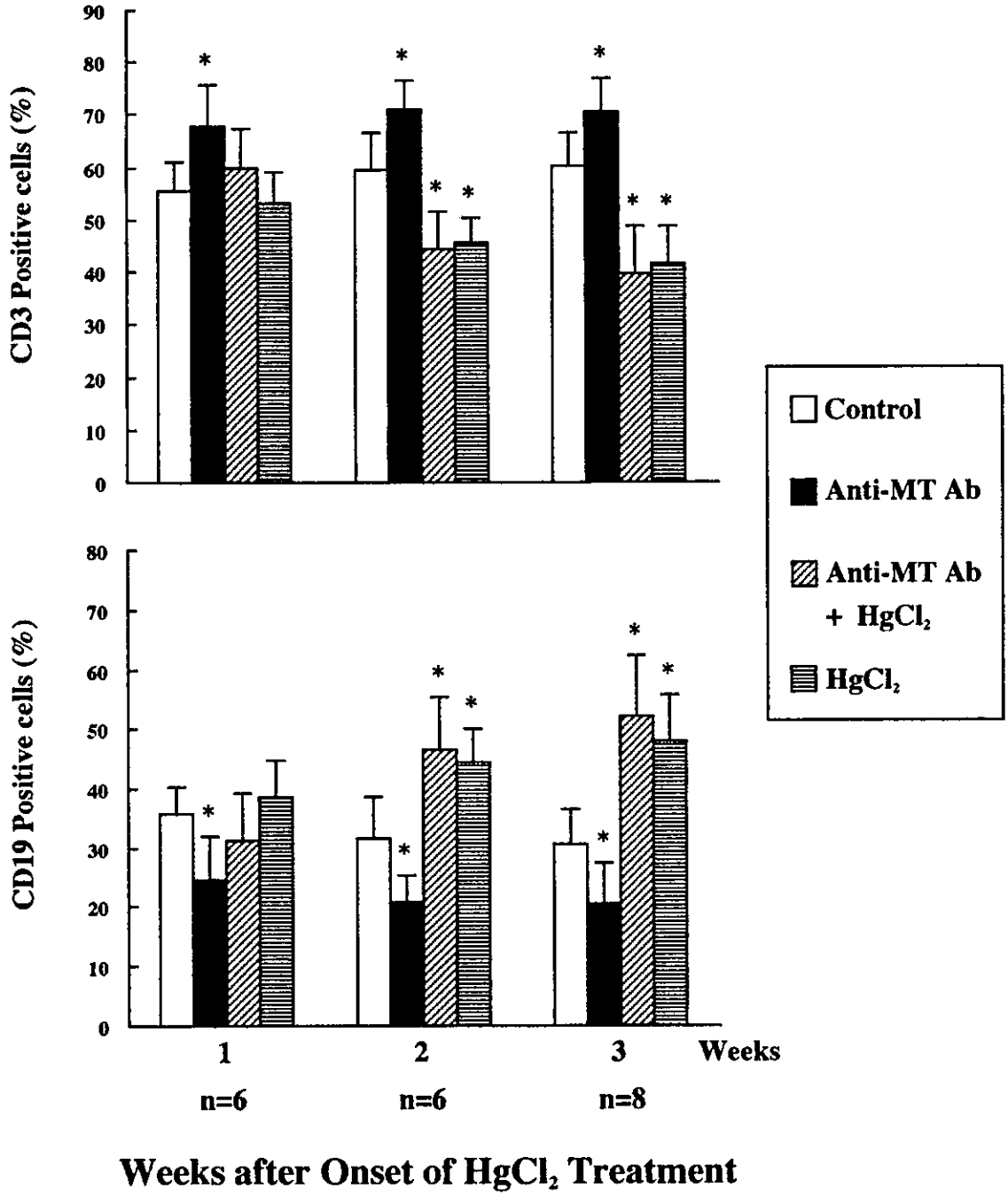

FIG. 8. Effects of MT immunization and $HgCl_2$ treatment on T and B cell percentages. Splenocytes were stained with FITC-conjugated anti-mouse CD19 and PE-conjugated anti-mouse CD3 mAbs. The CD3- and CD19-positive cell percentages were identified and quantified by flow cytometry analysis. Data are expressed as means ± SE. * $p < 0.05$, compared with control group.

such as mercury. Mercury can induce MT synthesis in liver and kidney (Sugawara *et al.*, 1998; Zalups and Koropatnick, 2000; Tandon *et al.*, 2001) and also lead to MT induction *in vitro* (Rodilla *et al.*, 1998; Schurz *et al.*, 2000). Since MT-null mice have been established (Michalska and Choo, 1993; Masters *et al.*, 1994a), many investigators are using MT-null mice to study the roles of MT in detoxification against heavy metals, including mercury.

Mercury shows toxic effects not only on the immune system, but also on other tissues. It has been reported that metallic mercury vapor causes pulmonary damage and that MT-null mice are more sensitive than wild-type mice (Yoshida *et al.*,

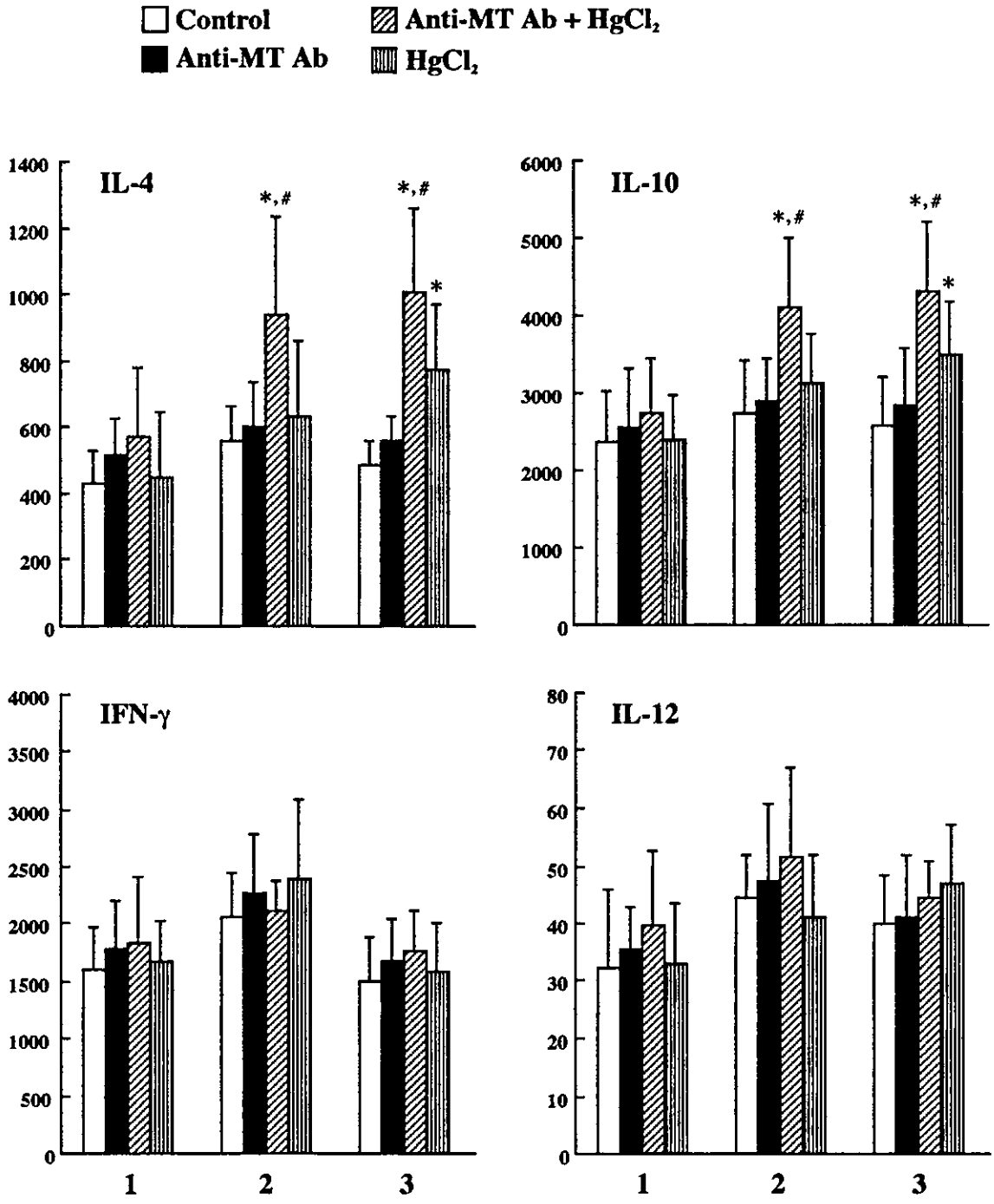

FIG. 9. Effects of MT immunization and $HgCl_2$ treatment on cytokine secretions (pg/ml). Splenic lymphocytes (2×10^6/ml) were *in vitro* stimulated by anti-mouse CD3 mAb (1 μg/ml) or LPS (10 μg/ml) for 24 h. The production of IL-4, IL-10, and IFN-γ in supernatants that were stimulated by anti-CD3 mAb, and IL-12 that was stimulated by LPS, were measured by using an ELISA method. Data are shown as means ± SE (n = 6–8). * $p < 0.05$, compared with control group; # $p < 0.05$, compared with $HgCl_2$ group.

1999). Inorganic mercury causes liver and kidney damage, but high intracellular levels of MT are capable of preventing the toxic effects of mercury (Morcillo and Santamaria, 1996; Sugawara *et al.,* 1998). Sensitivity to the renal toxicity of mercuric chloride was markedly enhanced in MT-null mice compared with wild-type mice (Satoh *et al.,* 1997). In this study, we observed that MT immunization impeded MT induction by $HgCl_2$ in the liver and enhanced mercury-induced immune disorders and liver injury, suggesting that anti-MT Ab induction enhances mercuric toxicity on the immune system and liver. Moreover, MT immunization also led to an increase of mercury levels in serum and liver, but a decrease in the kidney, suggesting that anti-MT Ab induction disturbs the excretion of mercury in mice. Further studies are needed to investigate whether anti-MT Ab induction enhances mercuric toxicity in other tissues.

Bone formation is mediated by osteoblasts, which are derived from mesenchymal stem cells present in the marrow stroma, which have the capacity to differentiate into fibroblasts, osteoblasts, and adipocytes. Osteoblast differentiation and maturation is an ordered process and expressed by osteoblast-specific markers, such as ALP and osteocalcin, and later mineral deposition (Stein *et al.,* 1990). ALP has been found to be expressed during the initial phase of osteoblast differentiation, before the appearance of a mineralized matrix (Owen *et al.,* 1990; Stein *et al.,* 1990; Malaval *et al.,* 1994; Yao *et al.,* 1994). Meanwhile, osteocalcin is expressed by relative mature osteoblasts during the terminal phase of osteoblast differentiation and after matrix mineralization (Owen *et al.,* 1990; Stein *et al.,* 1990; Kasugai *et al.,* 1991; Yao *et al.,* 1994). It has been reported that estrogen leads to increased femoral BMD and this is preceded by enhanced expression of ALP in mouse femurs (Plant and Tobias, 2001). In addition, C3H/HeJ (C3H) and C57BL/6J (B6) mice are similar in adult body size and have bones of similar external size. C3H mice have higher peaker bone density than B6 mice (Beamer *et al.,* 1996; Rosen *et al.,* 1997; Akhter *et al.,* 2000), and C3H mice have higher levels of serum ALP activity than B6 mice (Rosen *et al.,* 1997; Dimai *et al.,* 1998; Akhter *et al.,* 2000). A larger population of ALP-positive, osteoblast-lineage cells exist in the marrow of C3H compared with B6 mice (Dimai *et al.,* 1998), and a larger population of osteoclastic progenitor cells in the marrow of B6 animals compared with C3H mice is evident (Linkhart *et al.,* 1999). Furthermore, it has been reported that immunization with type II collagen in rats is a useful autoimmunity model of rheumatoid arthritis and also generalizes osteoporosis in juxtaarticular (Hanyu *et al.,* 1999). We examined systemic serum bone formation indices, ALP and osteocalcin, which reflect contributions from the total skeleton. Our results indicated that serum ALP activity and osteocalcin levels were significantly decreased in the MT immunization plus $HgCl_2$ treatment group compared with those in other groups. These results are consistent with those of a decrease in BMD. To our knowledge, there is no report that inorganic mercury causes bone injury in humans or experimental animals. In this study, $HgCl_2$ treatment alone did not cause any bone injury. However, when anti-MT Ab was induced in mice, mercury led to bone injury characterized by decreasing serum levels of ALP activity and osteocalcin. Therefore, we presume that anti-MT Ab induction in mice impedes MT induction by mercury in liver and may allow mercury to affect osteoblasts and thereby decrease BMD. Mercury-induced immune disorders may also be involved. Further studies are required to investigate whether these observations are related and to help describe the mechanisms involved in anti-MT Ab induction of mercury-induced decrease in BMD.

ACKNOWLEDGMENT

This work was supported in part by a grant-in-aid from Sanstar (Japan).

REFERENCES

Abedi-Valugerdi, M., and Möller, G. (2000). Contribution of H-2 and non-H-2 genes in the control of mercury-induced autoimmunity. *Int. Immunol.* **12,** 1425–1430.

Akhter, M. P., Iwaniec, U. T., Covey, M. A., Cullen, D. M., Kimmel, D. B., and Recker, R. R. (2000). Genetic variations in bone density, histomorphometry, and strength in mice. *Calcif. Tissue Int.* **67,** 337–344.

Bagenstose, L. M., Salgame, P., and Monestier, M. (1998a). Mercury-induced autoimmunity in the absence of IL-4. *Clin. Exp. Immunol.* **114,** 9–12.

Bagenstose, L. M., Salgame, P., and Monestier, M. (1998b). IL-12 down-regulates autoantibody production in mercury-induced autoimmunity. *J. Immunol.* **160,** 1612–1617.

Beamer, W. G., Donahue, L. R., Rosen, C. J., and Baylink, D. J. (1996). Genetic variability in adult bone density among inbred strains of mice. *Bone* **18,** 397–403.

Dastych, J., Walczak-Drzewiecka, A., Wyczolkowska, J., and Metcalfe, D. D. (1999). Murine mast cells exposed to mercuric chloride release granule-associated *N*-acetyl-β-D-hexosaminidase and secrete IL-4 and TNF-α. *J. Allergy Clin. Immunol.* **103,** 1108–1114.

Dimai, H. P., Linkhart, T. A., Linkhart, S. G., Donahue, L. R., Beamer, W. G., Rosen, C. J., Farley, J. R., and Baylink, D. J. (1998). Alkaline phosphatase levels and osteoprogenitor cell numbers suggest bone formation may contribute to peak bone density differences between two inbred strains of mice. *Bone* **22,** 211–216.

Doth, M., Fricke, M., Nicoletti, F., Garotta, G., Van Velthuysen, M. L., Bruijn, J. A., and Gleichmann, E. (1997). Genetic differences in immune reactivity to mercuric chloride ($HgCl_2$): Immunosuppression of $H\text{-}2^d$ mice is mediated by interferon-gamma (IFN-gamma). *Clin. Exp. Immunol.* **109,** 149–156.

Gillespie, K. M., Saoudi, A., Kuhn, J., Whittle, C. J., Druet, P., Bellon, B., and Mathieson, P. W. (1996). Th1/Th2 cytokine gene expression after mercuric chloride in susceptible and resistant rat strains. *Eur. J. Immunol.* **26,** 2388–2392.

Gorrie, M. J., Qasim, F. J., Whittle, C. J., Gillespie, K. M., Szeto, C. C., Nicoletti, F., Bolton, E. M., Bradley, J. A., and Mathieson, P. W. (2000). Exogenous type-1 cytokines modulate mercury-induced hyper-IgE in the rat. *Clin. Exp. Immunol.* **121,** 17–22.

Hanyu, T., Chotanaphuti, T., Arai, K., Tanaka, T., and Takahashi, H. E. (1999). Histomorphometric assessment of bone changes in rats with type II collagen-induced arthritis. *Bone* **24,** 485–490.

Hultman, P., and Enestrom, S. (1992). Dose–response studies in murine

mercury-induced autoimmunity and immune-complex disease. *Toxicol. Appl. Pharmacol.* **113,** 199–208.

Hultman, P., Turley, S. J., Enestrom, S., Lindh, U., and Pollard, K. M. (1996). Murine genotype influences the specificity, magnitude and persistence of murine mercury-induced autoimmunity. *J. Autoimmun.* **9,** 139–149.

Johansson, U., Hansson-Georgiadis, H., and Hultman, P. (1998). The genotype determines the B cell response in mercury-treated mice. *Int. Arch. Allergy Immunol.* **116,** 295–305.

Kasugai, S., Todescan, R. J., Nagata, T., Yao, K. L., Butler, W. T., and Sodek, J. (1991). Expression of bone matrix proteins associated with mineralized tissue formation by adult rat bone marrow cells *in vitro:* Inductive effects of dexamethasone on the osteoblastic phenotype. *J. Cell Physiol.* **147,** 111–120.

Linkhart, T. A., Linkhart, S. G., Kodama, Y., Farley, J. R., Dimai, H. P., Wright, K. R., Wergedal, J. E., Sheng, M., Beamer, W. G., Donahue, L. R., Rosen, C. J., and Baylink, D. J. (1999). Osteoclast formation in bone marrow cultures from two inbred strains of mice with different bone densities. *J. Bone Miner. Res.* **14,** 39–46.

Malaval, L., Modrowski, D., Gupta, A. K., and Aubin, J. E. (1994). Cellular expression of bone-related proteins during *in vitro* osteogenesis in rat bone marrow stromal cell cultures. *J. Cell Physiol.* **158,** 555–572.

Masters, B. A., Kelly, E. J., Quaife, C. J., Brinster, R. L., and Palmiter, R. D. (1994a). Targeted disruption of metallothionein I and II genes increases sensitivity to cadmium. *Proc. Natl. Acad. Sci. USA* **91,** 584–588.

Masters, B. A., Quaife, C. J., Erickson, J. C., Kelly, E. J., Froelick, G. J., Zambrowicz, B. P., Brinster, R. L., and Palmiter, R. D. (1994b). Metallothionein III is expressed in neurons that sequester zinc in synaptic vesicles. *J. Neurosci.* **14,** 5844–5857.

Michalska, A., and Choo, K. H. A. (1993). Targeting and germ line transmission of a null mutation at the metallothionein I and II loci in mouse. *Proc. Natl. Acad. Sci. USA* **90,** 8088–8092.

Morcillo, M. A., and Santamaria, J. (1996). Mercury distribution and renal metallothionein induction after subchronic oral exposure in rats. *Biometals* **9,** 213–220.

Oliveira, D. B., Gillespie, K., Wolfreys, K., Mathieson, P. W., Qasim, F., and Coleman, J. W. (1995). Compounds that induce autoimmunity in the Brown Norway rat sensitize mast cells for mediator release and interleukin-4 expression. *Eur. J. Immunol.* **25,** 2259–2264.

Owen, T. A., Aronow, M., Shalhoub, V., Barone, L. M., Wilming, L., Tassinari, M. S., Kennedy, M. B., Pockwinse, S., Lian, J. B., and Stein, G. S. (1990). Progressive development of the rat osteoblast phenotype *in vitro:* Reciprocal relationships in expression of genes associated with osteoblast proliferation and differentiation during formation of the bone extracellular matrix. *J. Cell Physiol.* **143,** 420–430.

Palmiter, R. D., Findley, S. D., Whitmore, T. E., and Durnam, D. M. (1992). MT-III, a brain-specific member of the metallothionein gene family. *Proc. Natl. Acad. Sci. USA* **89,** 6333–6337.

Park, J. D., Liu, Y., and Klaassen, C. D. (2001). Protective effect of metallothionein against the toxicity of cadmium and other metals. *Toxicology* **163,** 93–100.

Plant, A., and Tobias, J. H. (2001). Characterisation of the temporal sequence of osteoblast gene expression during estrogen-induced osteogenesis in female mice. *J. Cell Biochem.* **82,** 683–691.

Prigent, P., Saoudi, A., Pannetier, C., Graber, P., Bonnefoy, J. Y., Druet, P., and Hirsch, F. (1995). Mercuric chloride, a chemical responsible for T helper cell (Th)2-mediated autoimmunity in Brown Norway rats, directly triggers T cells to produce interleukin-4. *J. Clin. Invest.* **96,** 1484–1489.

Quaife, C. J., Findley, S. D., Erickson, J. C., Froelick, G. J., Kelly, E. J., Zambrowicz, B. P., and Palmiter, R. D. (1994). Induction of new metallothionein isoform (MT-IV) occurs during differentiation of stratified squamous epithelia. *Biochemistry* **33,** 7250–7259.

Rodilla, V., Miles, A. T., Jenner, W., and Hawksworth, G. M. (1998). Exposure of cultured human proximal tubular cells to cadmium, mercury, zinc and bismuth: Toxicity and metallothionein induction. *Chem.–Biol. Interact.* **14,** 71–83.

Rosen, C. J., Dimai, H. P., Vereault, D., Donahue, L. R., Beamer, W. G., Farley, J., Linkhart, S., Linkhart, T., Mohan, S., and Baylink, D. J. (1997). Circulating and skeletal insulin-like growth factor-I (IGF-I) concentrations in two inbred strains of mice with different bone mineral densities. *Bone* **21,** 217–223.

Satoh, M., Nishimura, N., Kanayama, Y., Nakanuma, A., Suzuki, T., and Tohyama, C. (1997). Enhanced renal toxicity by inorganic mercury in metallothionein-null mice. *J. Pharmacol. Exp. Ther.* **283,** 1529–1533.

Schurz, F., Sabater-Vilar, M., and Fink-Gremmels, J. (2000). Mutagenicity of mercury chloride and mechanisms of cellular defence: The role of metal-binding proteins. *Mutagenesis* **15,** 525–530.

Stein, G. S., Lian, J. B., and Owen, T. A. (1990). Relationship of cell growth to the regulation of tissue-specific gene expression during osteoblast differentiation. *FASEB J.* **4,** 3111–3123.

Sugawara, N., Lai, Y. R., Sugaware, C., and Arizono, K. (1998). Decreased hepatobiliary secretion of inorganic mercury, its deposition and toxicity in the Eisai hyperbilirubinemic rat with no hepatic canalicular organic anion transporter. *Toxicology* **126,** 23–31.

Tandon, S. K., Singh, S., Prasad, S., and Mathur, N. (2001). Hepatic and renal metallothionein induction by an oral equimolar dose of zinc, cadmium or mercury in mice. *Food Chem. Toxicol.* **39,** 571–577.

Urano, T., Hosoi, T., Shiraki, M., Toyoshima, H., Ouchi, Y., and Inoue, S. (2000). Possible involvement of the $p57^{Kip2}$ gene in bone metabolism. *Biochem. Biophys. Res. Commun.* **269,** 422–426.

Warfvinge, K., Hansson, H., and Hultman, P. (1995). Systemic autoimmunity due to mercury vapor exposure in genetically susceptible mice: Dose-response studies. *Toxicol. Appl. Pharmacol.* **2,** 299–309.

Wu, Z., Turner, D. R., and Oliveira, D. B. (2001). IL-4 gene expression up-regulated by mercury in rat mast cells: A role of oxidant stress in IL-4 transcription. *Int. Immunol.* **13,** 297–304.

Yao, K. L., Todescan, R. J., and Sodek, J. (1994). Temporal changes in matrix protein synthesis and mRNA expression during mineralized tissue formation by adult rat bone marrow cells in culture. *J. Bone Miner. Res.* **9,** 231–240.

Yoshida, M., Satoh, M., Shimada, A., Yasutake, A., Sumi, Y., and Tohyama, C. (1999). Pulmonary toxicity caused by acute exposure to mercury vapor is enhanced in metallothionein-null mice. *Life Sci.* **64,** 1861–1867.

Zalups, R. K., and Koropatnick, J. (2000). Temporal changes in metallothionein gene transcription in rat kidney and liver: Relationship to content of mercury and metallothionein protein. *J. Pharmacol. Exp. Ther.* **295,** 74–82.

Differential expression of secreted frizzled-related protein 4 in decidual cells during pregnancy

M Fujita[1,2], S Ogawa[1], H Fukuoka[2], T Tsukui[3], N Nemoto[4], O Tsutsumi[5,6], Y Ouchi[1] and S Inoue[1,3,6]

[1]Department of Geriatric Medicine, Graduate School of Medicine, University of Tokyo, 7–3–1, Hongo, Bunkyo-ku, Tokyo 113–8655, Japan

[2]Department of Developmental Medical Sciences, Institute of International Health, Graduate School of Medicine, University of Tokyo, 7–3–1, Hongo, Bunkyo-ku, Tokyo 113–0033, Japan

[3]Department of Biochemistry and Research Center for Genomic Medicine, Saitama Medical School, Morohongo, Moroyama-machi, Iruma-gun, Saitama 350–0495, Japan

[4]Department of Pathology, School of Medicine, Nihon University, 30–1, Oyaguchikami-machi, Itabashi-ku, Tokyo 173–8610, Japan

[5]Department of Obstetrics and Gynecology, Faculty of Medicine, University of Tokyo, 7–3–1, Hongo, Bunkyo-ku, Tokyo 113–8655, Japan

[6]CREST, Japan Science and Technology Corporation, Kawaguchi, Saitama 332–0012, Japan

(Requests for offprints should be addressed to S Inoue; Email: inoworld-tky@umin.ac.jp)

Abstract

During pregnancy, the uterus shows marked morphological and physiological changes under the regulation of ovarian steroid. To elucidate the molecular cues of these changes, we tried to identify the transcripts differentially expressed in the pregnant rat uterus by using the suppression subtractive hybridization method. Seven independent clones were isolated and one of the up-regulated genes was secreted frizzled-related protein 4 (sFRP4). sFRP4 contains a Wnt-binding domain and belongs to the secreted frizzled protein family whose members are assumed to function as modulators of the Wnt signal. The expression level of sFRP4 mRNA reached a peak in the pregnant uterus on day 12, when uterine decidualization was almost complete in the rat. *In situ* hybridization histochemistry revealed that sFRP4 transcripts were observed in the decidual cells. In addition, proliferating cell nuclear antigen (PCNA)-positive cells were shown to be overlapped in decidua, suggesting that sFRP4 mRNA expression was accompanied by the late phase of decidual cell proliferation. Moreover, sFRP4 and estrogen receptor-α transcripts were co-localized. Furthermore, we analyzed the regulation of sFRP4 by estrogen using 17β-estradiol-treated ovariectomized rats. sFRP4 mRNA was detected in the uterus at 48 h after estrogen treatment, especially in endometrial stroma where PCNA-positive cells were also observed. The results in this study led us to the notion that sFRP4 mRNA may be up-regulated after estrogen treatment in the late phase of uterine cell proliferation.

Journal of Molecular Endocrinology (2002) **28**, 213–223

Introduction

The uterus undergoes morphological and physiological changes during gestation to accommodate and protect the developing conceptus. Both estrogen and progesterone play important roles in this process, maintaining uterine quiescence during gestation and determining the onset of parturition (Fu *et al.* 1994, Chibbar *et al.* 1995, Hansen 1998, de Ziegler *et al.* 1998). To elucidate the molecular basis of these mechanisms, it is important to identify the genes and factors involved in the pregnant uterus. For example, the expression of collagen type I and III and fibronectin is increased in the myometrium of the pregnant uterus (Stewart *et al.* 1995), suggesting their physiological roles in the growth of the uterus during pregnancy. Several cytokines are also expressed in the pregnant uterus (Lim *et al.* 1998, Hatthachote & Gillespie 1999). Leukemia inhibitory factor, required for successful implantation, is secreted in the uterine endometrial gland (Charnock *et al.* 1994, Vogiagis & Salamonsen 1999). Macrophage-colony stimulating factor is widely distributed in the endometrium,

Journal of Molecular Endocrinology (2002) **28**, 213–223 Online version via http://www.endocrinology.org
0952–5041/02/028–213

decidua and placenta, suggesting its role in placental morphogenesis and trophoblast differentiation (Saito *et al.* 1994). It is well recognized that regulation of these factors provides a framework for understanding gestational changes of the uterus. Especially, the up-regulated genes during implantation and parturition are investigated because they are important for establishment of pregnancy and the onset of labor. However, relatively few factors up-regulated during the mid and late phase of pregnancy have been identified so far. During the later phase of pregnancy, the decidualization is completed and then decidual cell regression occurs (Ogle *et al.* 1999). In addition, myometrium is undergoing hypertrophy (Macphee & Lye 2000) accompanied by a significant increase of fetal mass (Dowell & Kauer 1997). To investigate the up-regulated genes in this period is important for understanding the precise mechanism of these changes.

In the present study, we tried to isolate the genes regulated in the later phase of the pregnant rat uterus, including downstream targets regulated by ovarian hormone, by using suppression subtractive hybridization (SSH) (Diatchenko *et al.* 1996). Here, we identified a predominant expression of the secreted frizzled-related protein 4 (sFRP4), a member of the secreted frizzled family, whose expression gradually elevated until mid-pregnancy. The distribution of sFRP4 transcripts was also examined by *in situ* hybridization histochemistry. To explore the possible role of sFRP4 expression in cell proliferation, co-localization of sFRP4 mRNA with proliferating cell nuclear antigen (PCNA) (Kelman & Hurwitz 1998, Tsurimoto 1998) in the uterus was analyzed. Then, we examined the hormonal regulation of sFRP4 expression in ovariectomized rats treated with 17β-estradiol.

Materials and methods

Animals and tissue preparation

Female 9-week-old Wistar rats with or without pregnancy were purchased from Charles River Japan (Tokyo, Japan). For pregnant rats, the day a vaginal plug was found was designated day 0, and rats on days 6, 9, 12 and 15 were used. The tissue preparation for Northern blot analysis was performed as follows. After surgical removal of the uteri under anesthesia, they were rapidly opened, and the pups and placenta were removed. The tissues were frozen in liquid nitrogen and stored at − 80 °C until RNA isolation. For *in situ* hybridization and immunohistochemistry, tissues were fixed with 4% paraformaldehyde in PBS and embedded in paraffin. The serial sections were cut and mounted on slides and stored at 4 °C. For estradiol treatment study, rats were ovariectomized. Two weeks after surgery, the rats received an s.c. injection of additional estradiol (10 μg/kg body weight) (Sigma, St Louis, MO, USA) suspended in olive oil and then killed 0, 2, 6, 24 and 48 h later. All animal studies followed the National Institutes of Health (NIH) guidelines for the Care and Use of Experimental Animals.

Total RNA and poly A+ RNA isolation

Total RNA was extracted from frozen non-pregnant and pregnant uteri using Isogen reagent (Nippon Gene, Tokyo, Japan). Poly A+ RNA was extracted from 250 μg total RNA using an Oligotex-dT30 mRNA purification kit (Takara Shuzo, Tokyo, Japan).

SSH

The subtraction cDNA library was made using a PCR-Select cDNA subtraction kit, according to the manufacturer's instruction (Clontech, Palo Alto, CA, USA). Briefly, poly A+ RNA obtained from day 15 pregnant uteri and non-pregnant uteri were designated as a tester and a driver respectively. The double-stranded cDNAs were synthesized from 2 μg of each poly A+ RNA. The synthesized double-stranded cDNAs were then digested with RsaI and ligated to adapters. Subtractive hybridizations were performed between the tester and the driver and the hybridization products were amplified by PCR (Diatchenko *et al.* 1999).

Sequences analysis

The amplified cDNA fragments from the secondary PCR were ligated into a pCRII vector using a T/A cloning kit (Invitrogen, Madison, WI, USA). Fifty clones were isolated and sequenced by an ALF auto sequencer (Pharmacia Biotech, Tokyo, Japan) with an Autoreading sequencing kit (Pharmacia Biotech). The retrieved sequences were aligned with cDNA sequences in the GenBank

nucleotide database at the National Center for Biotechnology Information (NIH, Bethesda, MD, USA) using the Blastn program to search for sequence matches (http://www.ncbi.nlm.nih.gov/blast/).

Northern blot analysis

Total RNA was prepared from non-pregnant uteri and pregnant uteri on days 6, 9, 12 and 15 as described above. Total RNA (20 μg/lane) was separated in 1% agarose gel. Northern blot analysis was performed as described previously (Ogawa *et al.* 1998). The sFRP4 cDNA fragment obtained by SSH and the glyceraldehyde-3-phosphate dehydrogenase (GAPDH) cDNA fragment (Orimo *et al.* 1995) were labeled with [α-^{32}P]dCTP using a BcaBEST Labeling kit (Takara Shuzo) and used as probes. Autoradiography was carried out at −80 °C with an intensifying screen for 48 h. The intensity of the hybridization band was measured using BioMax 1D image analysis software (Kodak, Rochester, NY, USA).

In situ hybridization histochemistry

Digoxigenin (DIG)-labeled single-stranded RNA probes were prepared using a DIG RNA labeling kit (Roche Diagnostics, Rotkreutz, Switzerland). The sFRP4 riboprobe was generated using a 474 bp cDNA fragment obtained by SSH. The estrogen receptor-α (ERα) riboprobe was generated from a 1803 bp full-length fragment containing the entire open reading frame of the receptor (Koike *et al.* 1987). *In situ* hybridization histochemistry was performed as described previously (Ishikawa *et al.* 1999). The sections were deparaffinized, rehydrated, incubated with 20 μg/ml proteinase K for 30 min at room temperature, treated with 0·2 M HCl for 10 min, and then acetylated. Hybridization was carried out at 55 °C for 18 h in a solution containing 25% formamide, 1·25 × SSC, 0·1% SDS, 50 μg/ml heparin, 50 μg/ml yeast RNA, and 1 μg/ml RNA probe. After washing twice with solution I (50% formamide, 5 × SSC, 1% SDS) at 55 °C for 30 min and three times with solution II (0·5 M NaCl, 10 mM Tris–HCl, 0·1% Tween 20) at room temperature for 10 min, the sections were treated with 25 μg/ml RNase A to remove non-specific binding of the probe. The sections were reacted with blocking solution containing casein (Roche Diagnostics) for 1 h, and incubated with alkaline phosphatase-labeled anti-DIG antibody for 18 h. The sections were washed and incubated with the chromogenic substrate solution containing 4-nitroblue tetrazolium chloride and 5-bromo-4-chloro-3-indolyl-phosphate (Roche Diagnostics) until adequate staining was observed.

Immunohistochemistry

PCNA was detected using immunohistochemical staining. After sections were hydrated, non-specific binding was blocked with PBS containing 10% fetal bovine serum (FBS) for 1 h. The sections were incubated with anti-PCNA mouse monoclonal antibody (Santa Cruz Biotechnology, Santa Cruz, CA, USA) or mouse IgG as a negative control diluted 1:500 in PBS containing 10% FBS for 18 h at 4 °C, followed by biotinylation with secondary antibody (anti-mouse rabbit immunoglobulins including IgG, IgA and IgM) for 1 h at room temperature. Sections were incubated with streptavidin conjugated with horseradish peroxidase and visualized by using peroxidase substrate 3,3′-diaminobenzidine (Histofine SAB-PO kit, DAB substrate kit; Nichirei Inc., Tokyo, Japan).

Results

Analysis of SSH PCR products

We selected fifty cDNA clones from the SSH cDNA library constructed between pregnant uteri on day 15 and non-pregnant uteri. The sequences were analyzed for similarity against all non-redundant database sequences using the gapped BLAST search. The isolated genes were summarized in Table 1. Some of the isolated clones corresponded to expressed sequence tags (ESTs). Seven differentially expressed clones were isolated from 50 clones and six out of seven clones were previously known genes that up-regulate during pregnancy, namely; α-2 macroglobulin (Fletcher *et al.* 1988, Thomas 1993), placental lactogen II (Faria *et al.* 1990), calcyclin (Thordarson *et al.* 1991, Waterhouse *et al.* 1992), plasma glutathione peroxidase (Takahashi *et al.* 1990), amiloride-binding protein (Lingueglia *et al.* 1993), and pregnancy-specific glycoprotein rnCGM (Chen *et al.* 1994). Interestingly, the last clone out of the

Table 1 Up-regulated genes in pregnant rat uterus isolated by suppression subtractive hybridization (SSH)

	cDNA	Localization	Day	Species	Reference
Novel	sFRP4	n.d.	n.d.	Rat	—
Known	α-2 Macroglobulin	Decidua, fetal liver	6–21	Rat	Fletcher *et al.* (1988) Thomas (1993)
	Placental lactogen II	Decidua, placenta, trophoblast giant cell	8–13	Mouse, rat	Faria *et al.* (1990)
	Calcyclin	Uterus, decidua, placenta	5–18	Mouse	Thordarson *et al.* (1991) Waterhouse *et al.* (1992)
	Plasma glutathione peroxidase	Placenta	n.d.	Human	Takahasshi *et al.* (1990)
	Amiloride-binding protein	Placenta	n.d.	Human, rat	Lingueglia *et al.* (1993)
	Pregnancy specific glycoprotein rnCGM3	Placenta	n.d.	Rat	Chen *et al.* (1994)
EST	EST 207450 (AI012999)	n.d.	n.d.	Rat	—
	EST 212820 (AI103531)	n.d.	n.d.	Rat	—

EST, expressed sequence tags; n.d.; not determined.

seven isolates was identical to sFRP4, which was identified as a novel up-regulated gene during pregnancy. sFRP4 is a member of the secreted frizzled-related protein family, and previously reported to be expressed in mammary gland, ovary and prostate (Wolf *et al.* 1997).

Since up-regulation of sFRP4 during pregnancy is a novel finding, we focused on sFRP4 for further study. sFRP4 contains a cysteine-rich domain (CRD) that functions as a Wnt-binding domain in frizzled proteins (Wolf *et al.* 1997). While frizzled proteins have a seven-pass transmembrane domain (Bhanot *et al.* 1996), secreted frizzled-related proteins including sFRP4 lack this domain.

The size of sFRP4 cDNA was reported to be 1910 nucleotides containing a 1044 bp open reading frame that encodes 348 amino acids (Wolf *et al.* 1997). The fragment size of our isolated fragment was 474 bp and corresponded to the fragment of nucleotides 661–1134 of sFRP4 cRNA (Wolf *et al.* 1997) (Fig. 1).

Expression of sFRP4 during pregnancy

To determine the expression pattern of sFRP4 mRNA during pregnancy, Northern blot analysis was performed for non-pregnant uteri and pregnant uteri on days 6, 9, 12 and 15. As shown in Fig. 2A, variable amounts of 2·0 kb and 2·9 kb sFRP4 mRNAs were detected in the pregnant uteri on days 9, 12 and 15. In contrast, sFRP4 mRNA was not detected in the pregnant uteri on day 6 and in non-pregnant uteri. The intensity of the hybridization bands was measured by a phosphor imager, and sFRP4 signals were normalized utilizing the GAPDH signals for each time point. The intensity of sFRP4 signal exhibited its peak on day 12 and declined gradually thereafter (Fig. 2B).

We further investigated the cell type-specific expression of sFRP4 in the pregnant uteri on day 12. *In situ* hybridization histochemistry revealed specific distributions of the sFRP4 transcripts, especially in the decidua and weakly in the myometrium (Fig. 3A). Control sections treated with sFRP4 sense probe showed no specific signals (Fig. 3B). In addition, the expression of ERα mRNA was investigated using an ERα-specific antisense probe. Although ERα mRNA was detected in the serosa, myometrium and decidua, strong signals were observed especially in the

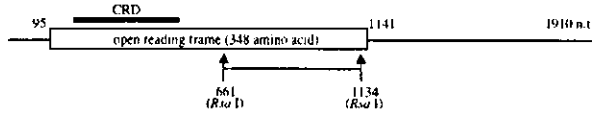

Figure 1 Isolated cDNA fragment of sFRP4. The size of the cDNA fragment was 474 bp and corresponded to the fragment of nucleotides 661–1134 of sFRP4 (Wolf *et al.* 1997). Both ends of the fragment contain RsaI sites because the synthesized double-stranded cDNA was digested with this restriction enzyme.

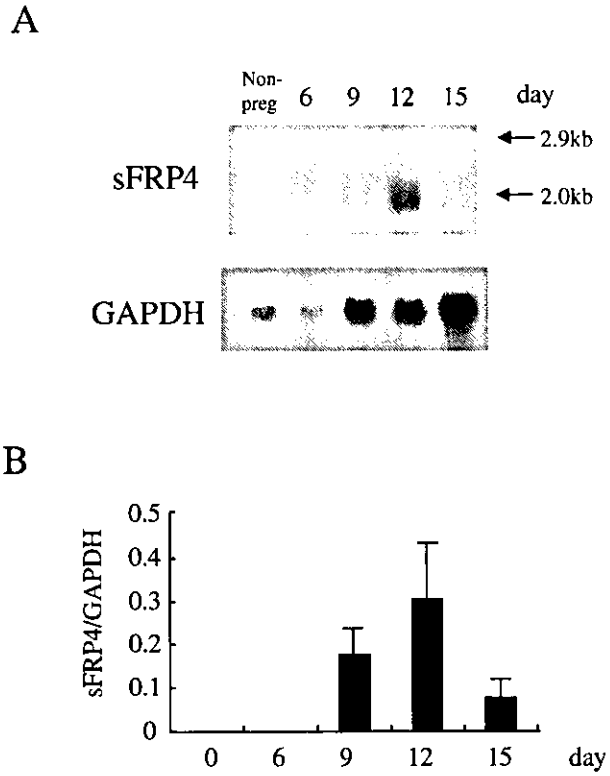

Figure 2 Expression of sFRP4 mRNA in rat uterus during pregnancy. (A) Northern blots containing total RNA (20 μg) extracted from non-pregnant (Non-preg) uteri and pregnant uteri on days 6, 9, 12 and 15 were hybridized with the sFRP4 cDNA probe or the GAPDH probe as an internal control. Variable amounts of 2·0 kb and 2·9 kb sFRP4 transcripts were detected in pregnant uteri on days 9, 12 and 15. In contrast, sFRP4 mRNA was not detected in non-pregnant uteri and pregnant uteri on day 6. (B) Semiquantitative analysis of the ratio of sFRP4 transcripts levels against GAPDH transcripts levels in pregnant uteri on days 9, 12, and 15 (n=3 for each group). Values are means±S.D.

decidua (Fig. 3C) where the sFRP4 transcripts were also detected (Fig. 3A). Control sections treated with ERα sense probe showed no specific signals (Fig. 3D). We further investigated whether expression of sFRP4 was involved in proliferation of deciduae using serial sections. As shown in Fig. 4A, a strong signal of sFRP4 was observed in the decidua. Distribution of PCNA-positive cells was overlapped in the decidua (Fig. 4C), suggesting that sFRP4 expression was observed in proliferating deciduae. There was no staining observed when the PCNA antibody was replaced by the mouse IgG (Fig. 4D).

Expression of sFRP4 by estrogen treatment

To investigate the possibility that sFRP4 is regulated by estrogen, the estrogen-treated ovariectomized rats were used as a model. Northern hybridization analysis revealed that the sFRP4 signal was detected in the uteri at 48 h after estrogen treatment. In contrast, sFRP4 mRNA was not detected in uteri at 0, 2, 6 and 24 h after estrogen treatment (Fig. 5A). No signal was observed at 0, 2, 6, 24 and 48 h after oil treatment (Fig. 5B). *In situ* hybridization histochemistry showed that sFRP4 mRNA was expressed predominantly in the endometrial stroma and less abundantly in the myometrium, whereas it was not detected in either luminal or glandular epithelium (Fig. 6A). The expression of sFRP4 in the endometrial stroma was observed more clearly by higher magnification (Fig. 6B). PCNA-positive cells were detected in the endometrial stroma, luminal epithelium and glandular epithelium (Fig. 6C).

Discussion

In the present study, using SSH we identified seven independent transcripts that up-regulated in the pregnant rat uterus. Six out of seven clones were previously known genes that up-regulate during pregnancy. One differentially expressed clone out of seven was found to be sFRP4 and this is the first report that sFRP4 is up-regulated during pregnancy. Amino acid sequences of sFRP4 proteins are well conserved among species. Rat sFRP4 was originally isolated from rat apoptotic tissues such as ovarian corpus luteum around parturition, involuted mammary gland and ventral prostate (Wolf *et al.* 1997, Guo *et al.* 1998). A human homologue of sFRP4 was identified as an up-regulated gene in endometrial carcinoma compared with normal endometrium (Abu-Jawdeh *et al.* 1999). A mouse homologue of sFRP4 was expressed in the developing teeth, eye and salivary gland of the embryo (Leimeister *et al.* 1998).

sFRP4 has a CRD, which functions as a Wnt-binding domain (Wolf *et al.* 1997). The Wnt family appears to induce multiple biological functions including cell growth, differentiation and survival (McMahon & Bradley 1990, Thomas & Capecchi 1990, Danielian & McMahon 1996). Wnt signal is transduced inside the cell by frizzled

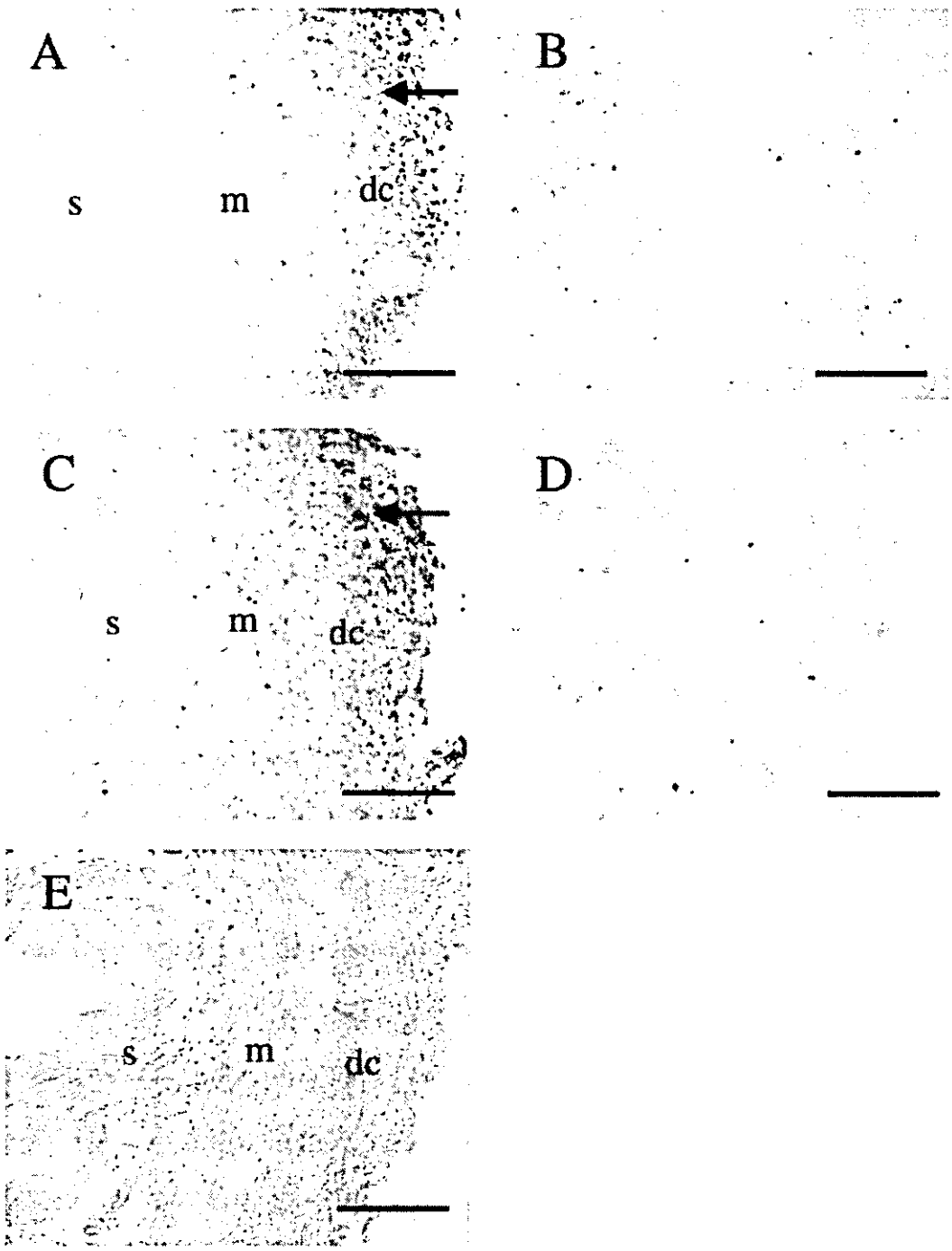

Figure 3 Distribution of sFRP4 mRNA and ERα mRNA in pregnant rat uteri on day 12. *In situ* hybridization histochemistry of sFRP4 (A, B) and ERα (C, D) and hematoxylin and eosin staining (E) were performed using pregnant uteri on day 12. (A) sFRP4 mRNA was detected in the decidua (dc) as indicated by the arrow when sFRP4-specific antisense RNA probe was used. (B) No signal was detected by sFRP4 sense probe. (C) ERα mRNA was detected especially in the decidua (dc) as indicated by the arrow when the ERα-specific antisense RNA probe was used. ERα mRNA was also observed in the myometrium (m) and serosa (s). (D) No signal was detected by the ERα sense probe. All experiments were performed three times. Bars=200 μm.

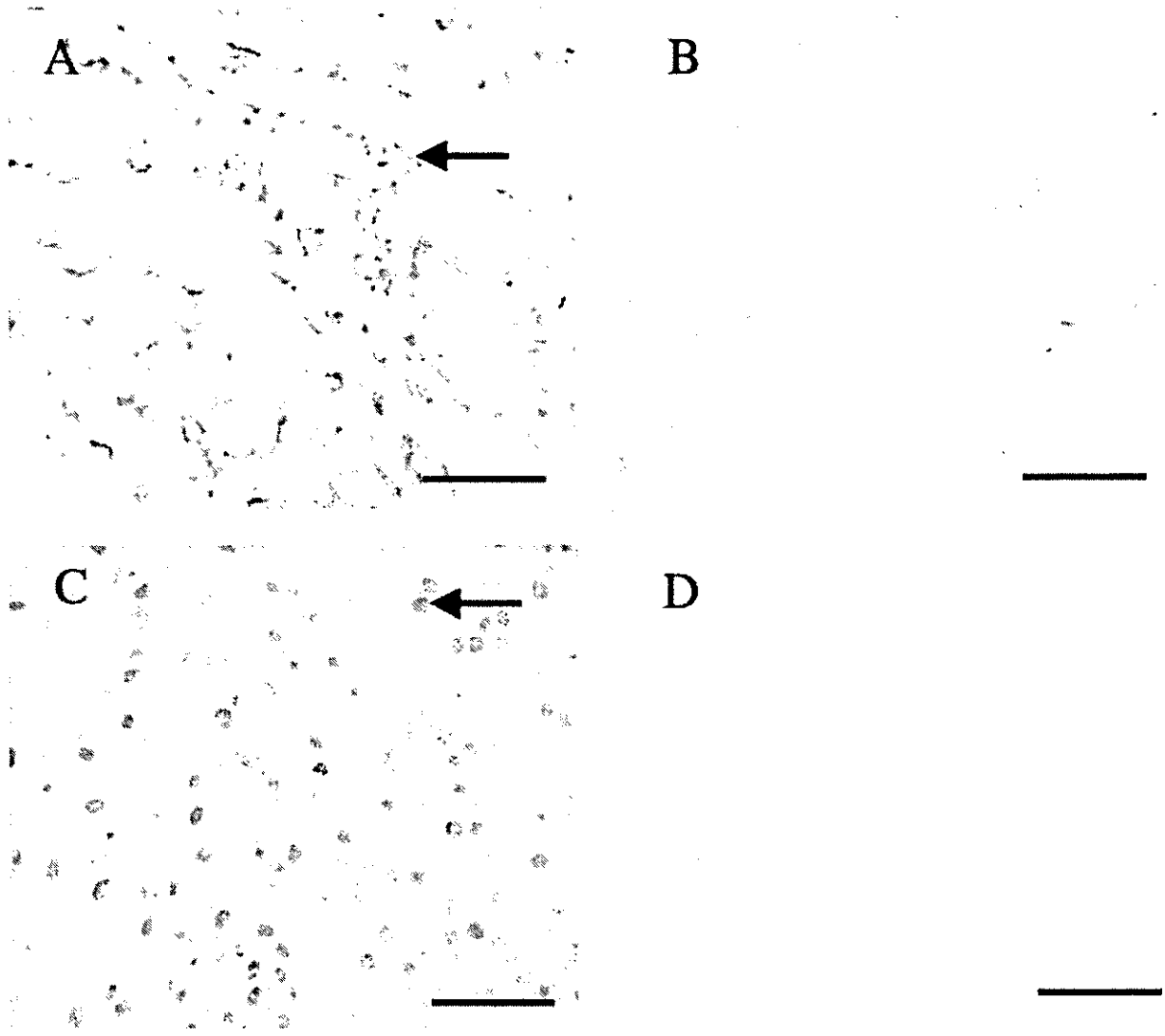

Figure 4 Proliferating cell nuclear antigen (PCNA)-positive cells were overlapped in the deciduae where sFRP4 mRNA was detected. *In situ* hybridization histochemistry of sFRP4 (A, B) and immunostaining of PCNA (C, D) were performed using serial sections of pregnant uteri on day 12. (A) Strong signal of sFRP4 mRNA was observed in the decidua. One of the positive signals of sFRP4 is marked with an arrow. (B) No signal was detected by sFRP4 sense probe. (C) PCNA-positive cells were also detected in the decidua. One of the positive signals for PCNA is marked with an arrow. (D) No signal was detected when mouse IgG was utilized. All experiments were performed three times. Bars=50 μm.

proteins, which contain a CRD and a seven-pass transmembrane domain (Bhanot *et al.* 1996). In contrast, secreted frizzled-related proteins, which possess a conserved CRD, lack the transmembrane domain. Although the biological activities of secreted frizzled proteins remain to be studied, they are assumed to function as modulators of the Wnt–frizzled signaling pathway. For example, it is reported that human frpHE antagonized the Wnt-8-mediated dorsal axis duplication in the *Xenopus* embryo (Abu-Jawdeh *et al.* 1999), suggesting that sFRP4 antagonizes Wnt signaling. In the rodent uterus, it is known that some Wnt genes such as *Wnt-4*, *-5a* and *-7a* are expressed (Miller *et al.* 1998). *Wnt-4* and *-5a* are expressed in the mouse uterine epithelium and stroma. *Wnt-7a* is expressed within the luminal epithelium. The expression levels of those Wnt genes in the uterus vary during the

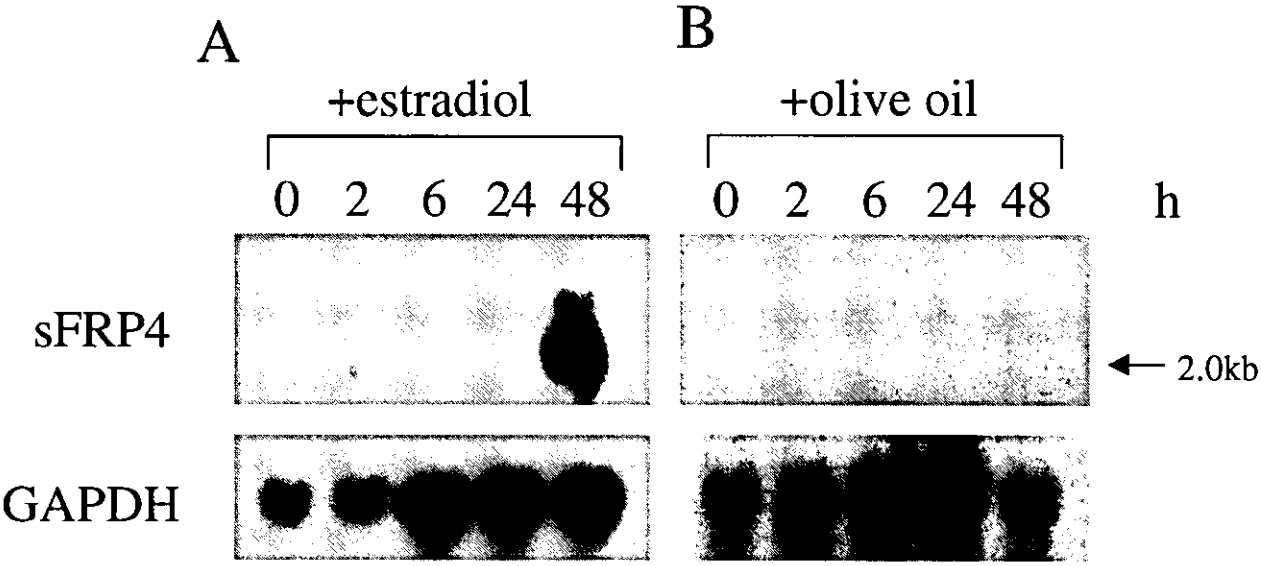

Figure 5 sFRP4 mRNA was regulated by estrogen in the uterus. Northern blots containing total RNA (20 μg) extracted from the ovariectomized rat uteri at 0, 2, 6, 24 and 48 h after estradiol treatment (10 μg/kg) or olive oil treatment were hybridized with the sFRP4 cDNA probe or the GAPDH probe as an internal control. (A) sFRP4 mRNA was detected only in the uterus at 48 h after the treatment. (B) No signal was detected after olive oil injection. All experiments were performed three times.

estrous cycle (Miller *et al.* 1998), suggesting that those expressions may be regulated by estrogen and play key roles in adult uterine function including the morphological changes which occur in response to circulating hormone levels (Miller & Sassoon 1998). It was also reported that the uteri of *Wnt-7a*-null mutant mice were smaller than that of wild type, absence of uterine glands and reduction in the mesenchymally derived stroma suggesting that *Wnt-7a* is required in cytodifferentiation in the uterus (Parr & McMahon 1998). During pregnancy, the expression of *Wnt-4* observed in the stroma surrounding the embryo at the onset of implantation and then the expression increased in the decidua (Paria *et al.* 2001). From the structural aspects of sFRP4, it is tempting to speculate that sFRP4 modulates the Wnt signal pathway via binding to some Wnt genes such as *Wnt-4*, *-5a* and *-7a*.

Northern blot analysis revealed that the expression of sFRP4 mRNA was highest in the pregnant uteri on day 12. *In situ* hybridization histochemistry demonstrated that sFRP4 mRNA expression was restricted to the decidual cells. Moreover, PCNA-positive cells were mainly found in the decidual cells, where sFRP4 mRNA was detected. In the pregnant rat, endometrial stromal cells begin to proliferate and differentiate to form decidual tissue after implantation on day 6 (Abrahamsohn & Zorn 1993), and proliferation continues until day 12 when decidualization completes (Ogle *et al.* 1998). Thus, it is possible that the marked increase of sFRP4 transcripts in the decidua on day 12 was accompanied by the late phase of decidual cell proliferation. Alternatively, it is known that internucleosomal DNA fragmentation in the decidua basalis begins in mid-pregnancy (Ogle *et al.* 1999). From day 14, the decidual tissue begins to regress to the end of pregnancy (Ogle *et al.* 1990, Gu *et al.* 1994). The controlled cell death of large numbers of decidual cells allows remodeling of the implantation chamber without disrupting the growth and development of the embryo or the integrity of the uterus (Welsh & Enders 1985). Another study indicated that DNA breakdown was first detected at day 10 and that it increased time-dependently (Gu *et al.* 1994, Moulton 1994). Taken together, it is possible that sFRP4 might be involved in the initiation of decidual apoptosis by modulating some Wnt signals.

ERα mRNA was detected in the decidua as well as sFRP4 mRNA. It is known that the steroid hormones such as estrogen and progesterone modulate the structure and function of the uterus during pregnancy through their nuclear receptors